New Journal and we have not received input yet 26 (2021) 101013

Contents lists available at ScienceDirect

Thermal Science and Engineering Progress

journal homepage: www.elsevier.com/locate/tsep

Heat transfer enhancement with pressure drop optimisation in a horizontal porous channel locally heated from below

Suha A. Mohammed [a], Gazy F. Al-Sumaily [b,c,*], Hayder A. Dhahad [a], Mark C. Thompson [c]

[a] Mechanical Engineering Department, University of Technology, Baghdad, Iraq
[b] Workshop and Training Centre, University of Technology, Baghdad, Iraq
[c] Department of Mechanical and Aerospace Engineering, Monash University, Victoria, Australia

ARTICLE INFO

Keywords:
Mixed convection
Laminar flow
Porous media
Channels

ABSTRACT

In this work, transient mixed convection heat transfer and fluid flow in a horizontal porous layer bounded by two impermeable plates with a localised heating from below is numerically studied. The study is conducted using the Brinkman–Forchheimer-extended Darcy model and the one-equation energy model based on the assumption of local thermal equilibrium. The effects of porosity (ε = 0.7–0.95) and permeability represented by Darcy number (Da = 0.1–100) are investigated for the following ranges of Richardson (Ri = 1–100) and Reynolds (Re = 0.1–50) numbers. The results show that the existence of the porous material increases Nusselt number, but does not change its trend with Reynolds number for all Richardson numbers. Interestingly, it is shown that unstable, oscillatory flow and temperature fields are generated in both empty and porous channels at higher Richardson number and/or higher Reynolds number. Also, both the heat transfer and the pressure drop are found to decrease as the porosity increases; however, the effect of Darcy number depends strongly on the range of Reynolds number.

1. Introduction

In recent times, optimisation of energy expending in many thermal systems is classified among the most important significant problems in industrial sector. The use of porous media in such systems has appeared as a good technology for promoting the heat transfer with high performance. In such media, the effectual communication districts between the solid matrix and the flowing fluid increases largely, producing a considerable augmentation in rates of heat transfer. In fact, this enhancement in heat transfer is ascribed to a combination of influences; including increased mixing, direct conduction through the solid matrix, and thinning the thermal and hydrodynamic boundary layers about the heat source. Importantly, the efficiency of heat transfer enhancement relies substantially on the fluid flow conditions and the structural and thermo-physical properties of the porous medium used. Indeed, nevertheless, the augmented heat transfer acquired due to the use of porous media is at the expense of a greatly raised disadvantageous pressure drop. Energy transport by mixed convection in porous channels can be found in different modern practical applications such as, but are not restricted to, heat sinks of micro-electronics, solar plants, electronic cooling devices, and compact heat exchangers, and has been a frequently investigated topic. The problem of mixed convection in a vertical porous channel has been thoroughly investigated in the literature by many researchers. Hadim and Chen [1] investigated the effects of Darcy number and asymmetric heating boundary condition for both uniform wall temperature and uniform wall heat flux. They found that the improvement in heat transfer within the mixed convection region is more vigorous in the uniform wall temperature condition. Chen et al. [2] examined both the buoyancy-opposed and the buoyancy-assisted forced flows in a vertical porous channel. The study indicated that Darcy number possesses a significant impact on Nusselt number. Rami et al. [3] studied the flow of Newtonian fluid inside a porous medium confined by a vertical plate at constant temperature and concentration. They reported a significant positive impact from the mixed convection parameter on the rates of mass and heat transfer because the momentum transport, which has the negative influence on the boundary layer thickness. Degan and Vasseur [4] tested upward assisted flow using both the simple Darcy model and the generalised Brinkman-extended-Darcy model. The study concluded that the results obtained from the later model are resembled to those given by the pure Darcy model for low porosity media. Pop et al. [5] studied the interaction between the fully developed flow and the heat transport inside a standing narrow duct packed with a porous material. They found

* Corresponding author at: Department of Mechanical and Aerospace Engineering, Monash University, Victoria, Australia.
E-mail addresses: 20050@uotechnology.edu.iq (S.A. Mohammed), gazy.alsumaily@monash.edu (G.F. Al-Sumaily), 10592@uotechnology.edu.iq (H.A. Dhahad), mark.thompson@monash.edu (M.C. Thompson).

https://doi.org/10.1016/j.tsep.2021.101013
Received 17 March 2021; Received in revised form 30 June 2021; Accepted 2 July 2021
Available online 17 July 2021
2451-9049/© 2021 Elsevier Ltd. All rights reserved.

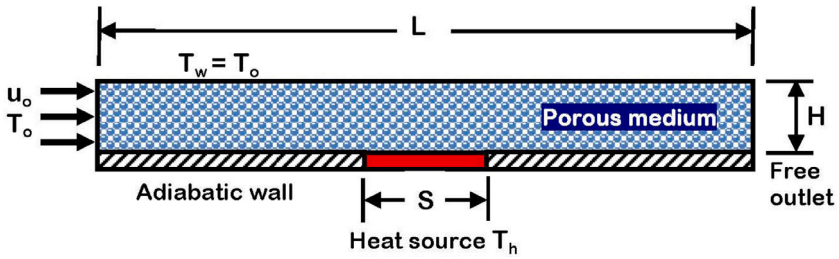

Fig. 1. Description of physical problem.

limited values of duct width and mixed convection parameter that have important effects on making recirculating flows through the duct. Umavathi et al. [6] examined mixed convection in a channel with symmetric and asymmetric walls for three various thermal wall conditions, i.e,. isothermal–isoflux, isoflux–isothermal, and isothermal–isothermal, using the full Brinkman–Forchheimer-extended Darcy model. It was found that the Forchheimer drag term has a major impact on the flow especially for unequally wall temperature, hence it reduces the flow field and generates flow reversal near the walls. Buonomo et al. [7] analysed transient mixed convection in an upward channel inserted with air-saturated aluminium foam partially heated from below, employing the Brinkman–Forchheimer-extended Darcy model and assuming the local thermal non-equilibrium condition in the porous channel. The results showed that all considered cases reach the steady state condition without oscillations. Avramenko et al. [8] studied mixed convection in vertical circular and flat micro-channels packed with a porous material, and subjected to slip boundary conditions. The results revealed that for weak heating condition, the reduction in Darcy number leads to an augmentation in heat transfer and an increase in the hydraulic resistance. However, for high heating condition, the trend of results turns into the opposite.

Later, Izadi et al. [9] tested mixed convective nanofluid flow in a $3D$ rectangular channel comprising carbon nanotubes. The results showed that the influence of the opposed buoyant forces is to decrease the flow velocity close to the channel walls, causing a considerable reduction in convection heat transfer. Kotresha and Gnanasekaran [10] and Kotresha et al. [11] studied mixed convective assisted flow throughout vertical channels filled with brass wire mesh and aluminium foam, respectively, of different porosities, using the Darcy–Forchheimer and the two-equations thermal models. In the former study, they found that the rate of heat transfer is enhanced by increasing the channel mesh filling. Hence, it was observed that Nusselt number increases from 60% to 88%, comparing to the case of entirely filling channel, by increasing the mesh filling from 40% to 70%, respectively, with 50% pressure drop less. In their later study, they predicted that the heat transfer rate enhances as the PPI of the aluminium foam increases. Thus, it was seen that the channel filled with 45 PPI foam transfers heat 1.77 times higher than that filled with 10 PPI foam. Leela et al. [12] examined buoyancy-assisted mixed convective flow in a vertical micro-porous-channel with viscous dissipation and interior heat generation under constant wall temperature and constant heat flux. The Darcy–Brinkman and the local thermal non-equilibrium models were employed to test the impact of main parameters like Rayleigh number, Brinkman number, Rayleigh number, thermal conductivity ratio, Darcy number, interfacial heat transfer coefficient, and solid internal heat generation. It was found that the increase in the interior heat generation, Rayleigh number, or Brinkman number increases Nusselt number; however, the interfacial coefficient decreases it, while Nusselt number was shown to be not affected by Darcy number. Manish et al. [13] and Shankar et al. [14] reported stability analyses of mixed convective flows in vertical channels differentially heated and filled with oil-saturated and water-saturated porous materials.

Moreover, the case of mixed convection in a horizontal channel filled with a porous medium has been frequently investigated in the literature. Lai et al. [15] investigated the impact of heat source size on the flow structure, thermal field, and heat transfer rates inside a horizontal porous channel heated partially from below. The results showed that for small Rayleigh numbers, the characteristics of the temperature and flow fields are basically the same for any size of heat source. However, for high Rayleigh numbers, recirculating cells are generated, and a flow transition from a multi-cellular to a bi-cellular region is observed depending on the value of Péclet number. Prasad et al. [16] extended the work of Lai et al. [15] by investigating the steady interaction mechanism between the buoyant effects and the forced flow when the width of the heat source is equivalent to the height of the horizontal porous layer. The results revealed that the externally stimulated flow field is considerably disturbed by an increase in Rayleigh number, producing bi-cellular recirculating flows in the proximity of the heat source. Another important aspect of buoyant influences is displayed at high Rayleigh number and low Péclet number, where multiple secondary cells might appear by the reason of reducing the intensity of forced flow. Chou and Chung [17] studied non-Darcian mixed convection in three horizontal square packed-sphere beds; water–stainless steel spheres bed, air–glass spheres bed, and water–glass spheres bed, for both uniform axial heat flux and uniform circumferential wall temperature. The results disclosed a significant influence from buoyancy forces on the structure of secondary flows and the rates of heat transfer at low Péclet number and low thermal conductivity ratio; however, the buoyancy effect is suppressed when any one of these parameters increases. Yokoyama et al. [18] examined steady mixed convection in a water-saturated horizontal packed bed of spherical glasses, employing Darcy and non-Darcian formulations. The cross-sectional area of the bed has an abrupt expansion step, with a heat source positioned on the base surface downstream and directly neighbouring to the step. The results predicted that heat transfer is unaffected by the existence of the expansion step, in comparison with the case of a bed without step, and inclusion of non-Darcy effects. Chang et al. [19] studied non-Darcian mixed convection in a square channel packed with stainless steel spheres under uniform axial heat flux. It was shown that secondary flows stimulated by buoyancy effects become more powerful and heat transfer is greater by decreasing Péclet number and increasing Rayleigh number. Cimpean et al. [20] reported an analytical analysis for steady mixed convection inside an inclined porous channel under a constant heat flux on each surface. They tested the effect of inclination angle changing from when the channel is in a vertical upwards direction to the horizontal situation. The study found that increasing Péclet number decreases the inclination effect and generates more symmetrical solution. Wong and Saeid [21] investigated the effects of inertial coefficient and porosity on mixed convection in a horizontal porous channel heated isothermally from below by a heat source that is cooled by an air jet impingement. They found that in the Darcy regime, the inertial coefficient and the porosity have insignificant impacts on Nusselt number. However, in the non-Darcy regime, these effects become merely important when the forced convection mode dominates, wherein the increment in anyone of them reduces Nusselt number. Dixon and Kulacki [22] measured experimentally the heat transfer coefficient of mixed convection in a packed bed of glass beads, heated from below by a finite-length heat source. They formulated a correlation for Nusselt number in terms of Péclet number, Rayleigh–Darcy number,

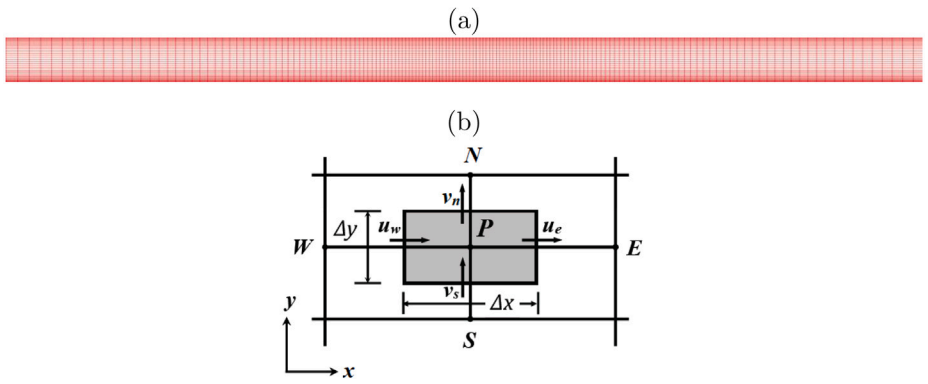

Fig. 2. (a) The computational domain used in the study. (b) Typical control volume surrounding a main grid node P, and demonstrating the staggered locations.

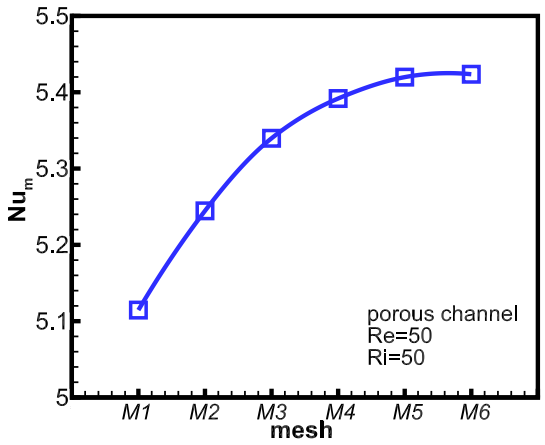

Fig. 3. Results of Nu_m for the grid resolution study.

and the bed thickness, in an attempt to validate their prior numerical predictions published in Dixon and Kulacki [23]. Following, Ozgen and Yasin [24] examined the effect of heat source position on steady mixed convection in a horizontal porous channel heated from below, by sliding it to the up-stream and down-stream of the channel equally. The results displayed complex secondary flows induced as the buoyancy effect increases, producing an increase in Nusselt number. As a result, they claimed that the two dimensional laminar flow changes into a three-dimensional flow. Barletta and Rees [25] and Barletta et al. [26] analysed the linear buoyancy-induced instability of mixed convective flows in horizontal porous channels employing the Darcy–Forchheimer formulation. Buonomo et al. [27] carried out experimental and numerical investigations on mixed convective air-flow in a horizontal channel subjected to a constant heat flux from below, and stuffed with an aluminium foam. The results indicated that employing aluminium foam augments the rate of heat transfer promoting a high level of surface heat dissipation. There have been very few attempts in the literature to study transient behaviour of mixed convective flow in horizontal porous channels. Thus, Lai and Kulacki [28] investigated such phenomenon with heating the lower wall isothermally, and pointed out that when the length of the heat source is larger than three times the height of the porous layer, using a steady-state numerical analysis and applying the convergence criteria become inappropriate for analysing such case for leading to a converged solution. They observed a high level of oscillation in the flow and temperature fields, particularly for high Rayleigh and Péclet numbers. Therefore, instead, they recommended to consider a transient analysis for the purpose of analysing this phenomenon any further. Saeid and Pop [29], studied similar case as Lai and Kulacki [28] but for isoflux heating source for three sizes of heater and at different Péclet numbers. The results showed that only for moderate values of Péclet number, when the mixed convection mode is dominated, oscillatory convective flows were observed, and a periodic variation of Nusselt number was obtained. They indicated that this oscillation is owing to the balance of the external flow effects and the buoyancy-induced effects inside the channel. However, both of these studies used the simple Darcy model to simulate the flow field without inclusion the non-Darcy effects. Indeed, in the non-Darcy regime, when the forced or mixed convection mode dominates, these effects become very significant. Therefore, in the present study, we employed the full Brinkman–Forchheimer-extended Darcy model to consider further investigation for the case studied previously by Lai and Kulacki [28] and Saeid and Pop [29]. Thus, numerical analysis of transient mixed convective fluid flow and heat transfer in a horizontal porous layer confined by two impermeable walls, and subject to a wide-size localised heating from the bottom wall, is conducted to develop a better understanding of the time-dependent interaction between the buoyancy-induced effects, which is developing timely, and the forced flow effects. In addition, according to the prior research, putting a large volume of porous material in any thermal convective application is the prime reason of raising the pressure drop. Therefore, the second innovation of the present work is to inspect the influences of porous media properties, in particular the porosity and the permeability, and find out more efficient technique to optimise the heat enhancement and the pressure drop.

2. Description of Physical problem and formulation

The geometry under consideration, shown in Fig. 1, is a two-dimensional horizontal porous layer confined by two impermeable stationary plates, isothermally heated from below by a finite heat source at constant temperature T_h. The porous layer, which is considered to have a height of H and a length of $L = 21H$, is made of an aluminium fibrous foam with a thermal conductivity of $k_s = 237$ W/m K, and is assumed to be fully saturated by air with a thermal conductivity of $k_f = 0.02587$ W/m K; hence, the solid-to-fluid thermal conductivity ratio becomes $k_r = (k_s/k_f) = 0.916\times10^4$. The influence of the structural properties of the porous medium employed such as the porosity ε and the permeability K will be tested in the current investigation. The size of the heat source is considered to be three times the layer height $S = 3H$, and the rest of the lower plate is insulated, whereas the upper plate is kept at an unchanging cooled temperature $T_w = T_o$. For mixed convection, a uniform flow of steady velocity u_o and constant temperature T_o is provoked to enter the layer from the away left leading edge as a result of a hydrostatic pressure difference.

The fluid flow field is calculated based on the Brinkman-Forchheimer-extended Darcy model, which involves the effects of the viscous drag and the inertia forces. Whereas, the temperature field is estimated based on the one-equation energy model (*Local Thermal*

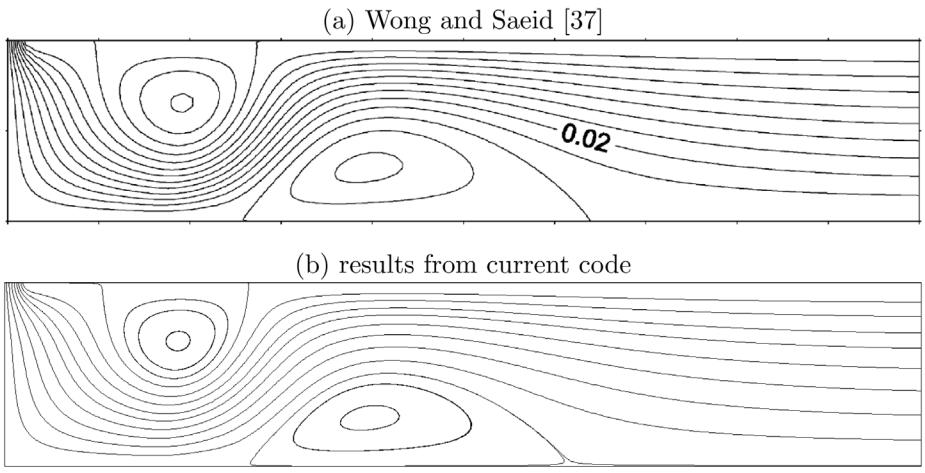

Fig. 4. Comparison between the results of Wong and Saeid [30] (Top) and those estimated by the current code (Bottom), for streamlines of an air jet impingement cooling of a heat source embedded in a porous channel at Péclet number Pe = 40.

Equilibrium model – LTE), which considers the thermal equilibrium condition between the fluid and the solid phases. Therefore, accordingly, the $2D$ dimensional governing equations for a transient, laminar, newtonian, incompressible, mixed convective flow, which invokes the Boussinesq approximation, can be expressed, as follows (Kaviany [31] and Nield and Bejan [32]):

$$\frac{\partial u}{\partial x}+\frac{\partial v}{\partial y}=0, \tag{1}$$

$$\frac{\rho_f}{\varepsilon}\left(\frac{\partial u}{\partial t'}\right)+\frac{\rho_f}{\varepsilon^2}\left(u\frac{\partial u}{\partial x}+v\frac{\partial u}{\partial y}\right)=-\frac{\mu_f}{K}u-\frac{\rho_f C_F\varepsilon}{\sqrt{K}}\left|\vec{\mathbf{u}}\right|u+\frac{\mu_f}{\varepsilon}\left(\frac{\partial^2 u}{\partial x^2}+\frac{\partial^2 u}{\partial y^2}\right)-\frac{\partial p_f}{\partial x}, \tag{2}$$

$$\frac{\rho_f}{\varepsilon}\left(\frac{\partial v}{\partial t'}\right)+\frac{\rho_f}{\varepsilon^2}\left(u\frac{\partial v}{\partial x}+v\frac{\partial v}{\partial y}\right)=-\frac{\mu_f}{K}v-\frac{\rho_f C_F\varepsilon}{\sqrt{K}}\left|\vec{\mathbf{u}}\right|v+\frac{\mu_f}{\varepsilon}\left(\frac{\partial^2 v}{\partial x^2}+\frac{\partial^2 v}{\partial y^2}\right)-\frac{\partial p_f}{\partial y}+\rho_f\beta_f g\left(T-T_o\right), \tag{3}$$

where,

$$\left|\vec{\mathbf{u}}\right|=\sqrt{u^2+v^2},$$

$$\left(\rho c_p\right)_m\left(\frac{\partial T}{\partial t'}\right)+\varepsilon\left(\rho c_p\right)_f\left(u\frac{\partial T}{\partial x}+v\frac{\partial T}{\partial y}\right)=\left[\frac{\partial}{\partial x}\left(k_{f.\mathrm{eff}}\frac{\partial T}{\partial x}\right)+\frac{\partial}{\partial y}\left(k_{f.\mathrm{eff}}\frac{\partial T}{\partial y}\right)\right], \tag{4}$$

where,

$$\left(\rho c_p\right)_m=\varepsilon\left(\rho c_p\right)_f+\left(1-\varepsilon\right)\left(\rho c_p\right)_s,$$

here, u and v are the horizontal and vertical fluid velocities, respectively; p_f and T are the fluid pressure and temperature, respectively; and t' is the time variable. Also, c_p, μ_f, $k_{f.\mathrm{eff}}$, and ρ_f refer to the fluid properties, e.g., specific heat, dynamic viscosity, effective thermal conductivity, and density, respectively. Whereas, C_F, K, and ε are the inertia coefficient, the permeability, and the porosity of the porous medium, respectively. The subscripts f and s denote to the fluid and solid phases, respectively. For analysing the problem in a general scale, the following non-dimensional scaling parameters are employed:

$$U=\frac{u}{u_o},\quad V=\frac{v}{u_o},\quad X=\frac{x}{H},\quad Y=\frac{y}{H},\quad P_f=\frac{p_f}{\rho u_o^2},\quad t=\frac{t'}{u_o H},$$

$$\theta=\frac{(T-T_o)}{(T_h-T_o)}. \tag{5}$$

Using these parameters in Eq. (5) into the aforementioned dimensional Eqs. (1)–(4), the following non-dimensional equations are developed, which was also justified in our prior work (Wissam et al. [33]):

$$\frac{\partial U}{\partial X}+\frac{\partial V}{\partial Y}=0, \tag{6}$$

$$\left(\frac{\partial U}{\partial t}\right)+\frac{1}{\varepsilon}\left(U\frac{\partial U}{\partial X}+V\frac{\partial U}{\partial Y}\right)=-\frac{\varepsilon}{\mathrm{Re.Da}}U-\frac{\varepsilon^2.C_F}{\sqrt{\mathrm{Da}}}\left|\vec{\mathbf{U}}\right|U+\frac{1}{\mathrm{Re}}\left(\frac{\partial^2 U}{\partial X^2}+\frac{\partial^2 U}{\partial Y^2}\right)-\varepsilon\left(\frac{\partial P_f}{\partial X}\right), \tag{7}$$

$$\left(\frac{\partial V}{\partial t}\right)+\frac{1}{\varepsilon}\left(U\frac{\partial V}{\partial X}+V\frac{\partial V}{\partial Y}\right)=-\frac{\varepsilon}{\mathrm{Re.Da}}V-\frac{\varepsilon^2.C_F}{\sqrt{\mathrm{Da}}}\left|\vec{\mathbf{U}}\right|V+\frac{1}{\mathrm{Re}}\left(\frac{\partial^2 V}{\partial X^2}+\frac{\partial^2 V}{\partial Y^2}\right)-\varepsilon\left(\frac{\partial P_f}{\partial Y}\right)+\varepsilon\mathrm{Ri}\;\theta, \tag{8}$$

where,

$$\left|\vec{\mathbf{U}}\right|=\sqrt{U^2+V^2},$$

$$\left(\frac{\partial\theta}{\partial t}\right)+\frac{\varepsilon}{C}\left(U\frac{\partial\theta}{\partial X}+V\frac{\partial\theta}{\partial Y}\right)=\frac{1}{C.\mathrm{Re.Pr}}\left[\frac{\partial}{\partial X}\left(k_{f.\mathrm{eff}}\frac{\partial\theta}{\partial X}\right)+\frac{\partial}{\partial Y}\left(k_{f.\mathrm{eff}}\frac{\partial\theta}{\partial Y}\right)\right], \tag{9}$$

where,

$$C=\varepsilon+\left(1-\varepsilon\right)\left(\frac{k_r}{\alpha_r}\right),$$

where, U, V are the non-dimensional velocity components along the directions X and Y, respectively; whereas θ, P_f and t are the non-dimensional temperature, pressure, and time, respectively. k_r and α_r are the solid/fluid thermal conductivity ratio and the solid/fluid thermal diffusivity ratio, respectively. By neglecting the dispersion conductivity, the effective fluid thermal conductivity represents only the stagnant conductivity, which is the product of the thermal conductivities of both solid and fluid phases and their phase fractions, suggested by Zehner and Schluender [34] as follows:

$$k_{f.\mathrm{eff}}=k_f\times\left(\left(1-\sqrt{1-\varepsilon}\right)+\frac{2\sqrt{1-\varepsilon}}{1-\lambda B}\times\left(\frac{(1-\lambda)B}{(1-\lambda B)^2}\ln(\lambda B)-\frac{B+1}{2}-\frac{B-1}{1-\lambda B}\right)\right), \tag{10}$$

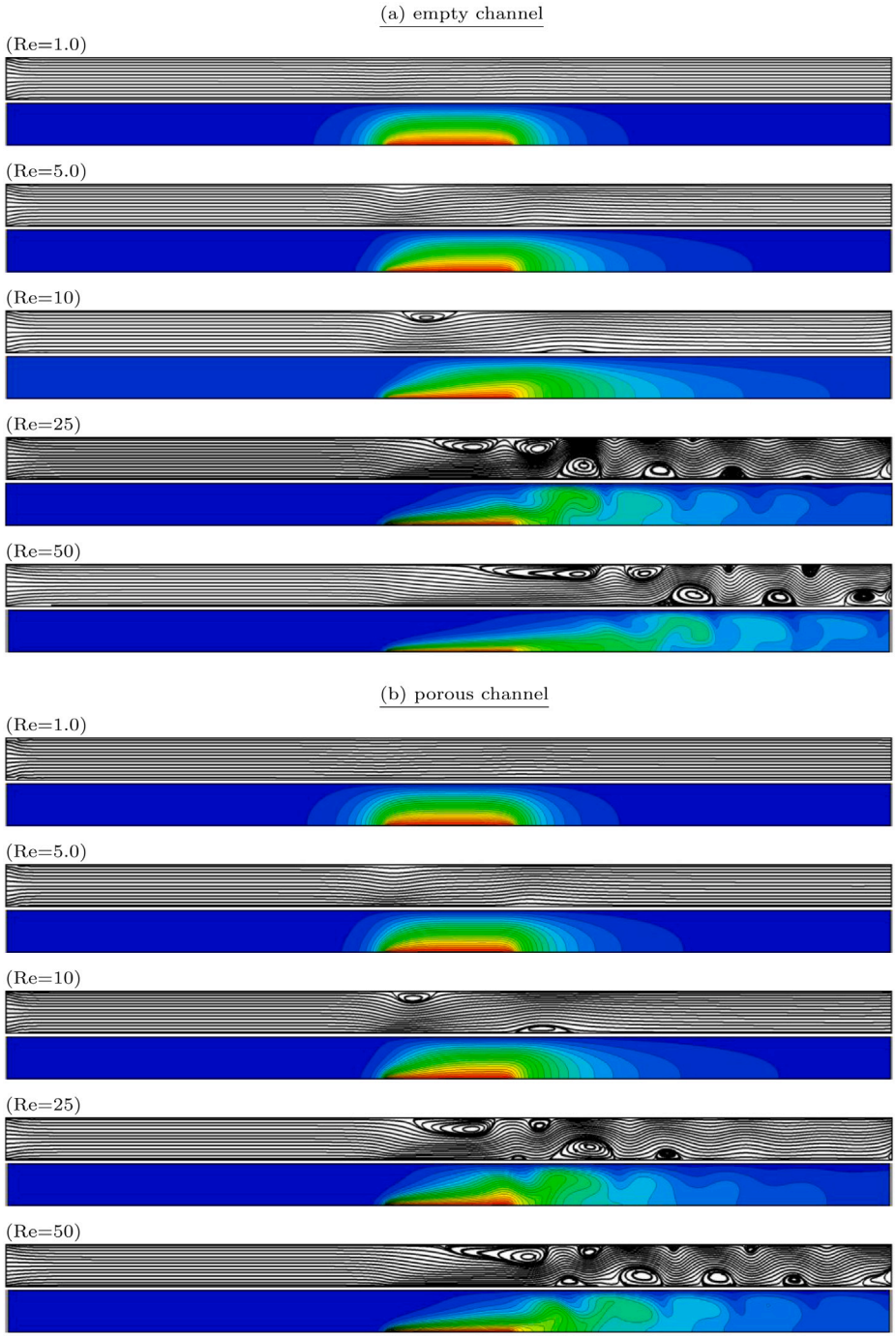

Fig. 5. Streamlines and isotherms patterns in both (a) empty and (b) porous channels, at Ri = 50, for different Re.

where,

$$\lambda = \frac{1}{k_r}, \quad B = 1.25\left(\frac{(1-\varepsilon)}{\varepsilon}\right)^{\frac{10}{9}}.$$

The inertia coefficient C_F in the momentum Eqs. (7) and (8) above is according to the practical correlation reported by Ergun [35], which is expressed in terms of the porosity ε of the porous medium as follows:

$$C_F = \frac{1.75}{\sqrt{150\varepsilon^3}}. \tag{11}$$

The pertinent variables that govern the present problem are Richardson number (Ri), Reynolds number (Re), Grashoff number (Gr), and Darcy number (Da), which can be defined as:

$$\mathrm{Ri} = \frac{\mathrm{Gr}}{\mathrm{Re}^2}, \quad \mathrm{Re} = \frac{u_o \rho_f H}{\mu_f}, \quad \mathrm{Gr} = \frac{g.\beta_f.\rho_f^2.H^3(T_h - T_o)}{\mu_f^2}, \quad \mathrm{Da} = \frac{K}{H^2}, \tag{12}$$

here, μ_f and ρ_f are the fluid dynamic viscosity and density, respectively.

The Brinkman–Forchheimer-extended Darcy momentum Eqs. (7) and (8) are converted into the standard Navier–Stokes equation by assuming the porosity $\varepsilon = 1$, as well as the permeability $K = \infty$ in Darcy number, and the LTE equation model (9) into the standard energy equation by assuming $C = 1$ and $k_{f.\mathrm{eff}} = k_f$, to calculate the velocity and temperature fields, respectively, in the empty channel

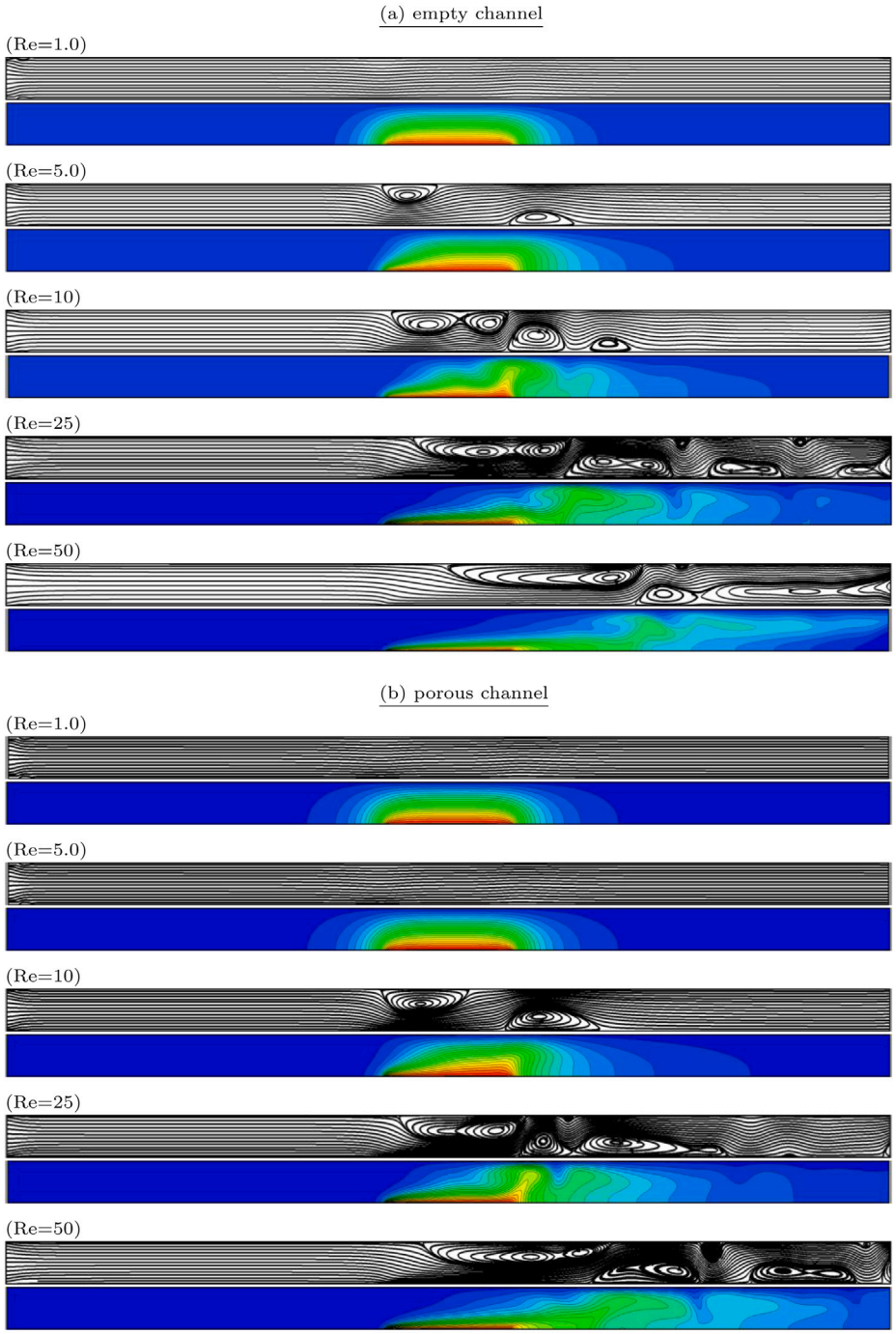

Fig. 6. Streamlines and isotherms patterns in both (a) empty and (b) porous channels, at Ri = 100, for different Re.

without the porous medium. Dirichlet boundary conditions, for the velocity and temperature, are enforced on the solid boundaries and at the inlet, whereas Neumann boundary conditions are enforced at the outlet. Thus corresponding initial and boundary conditions imported to the governing equations are:

$U = V = \theta = 0$, everywhere in the domain at $t = 0$.

Inlet, $U_o = 1,\ V_o = 0,\ \theta_o = 0,$

outlet, $\partial U/\partial X = \partial V/\partial X = \partial\theta/\partial X = 0,$

hot element, $U = V = 0,\ \theta_h = 1,$

bottom wall excepting heat source, $U = V = 0,\ \partial\theta/\partial Y = 0,$

top wall, $U = V = 0,\ \theta_w = \theta_o = 0.$ (13)

The local and average Nusselt numbers Nu_l and Nu_m, respectively, are calculated by the following formulae:

$$\mathrm{Nu}_l = \frac{h_x.Y}{k_f} = \frac{-k_{f.\mathrm{eff}}}{k_f}.\frac{(\partial T/\partial n).Y}{(T_h - T_o)} = \frac{-k_{f.\mathrm{eff}}}{k_f}.\frac{\partial\theta}{\partial n}\bigg|_h, \tag{14}$$

$$\mathrm{Nu}_m = \frac{1}{S}\sum\int_0^S \mathrm{Nu}_l.dn \tag{15}$$

where h_x is the localised convection heat transfer coefficient in X-direction, n is the perpendicular direction to the horizontal hot segment.

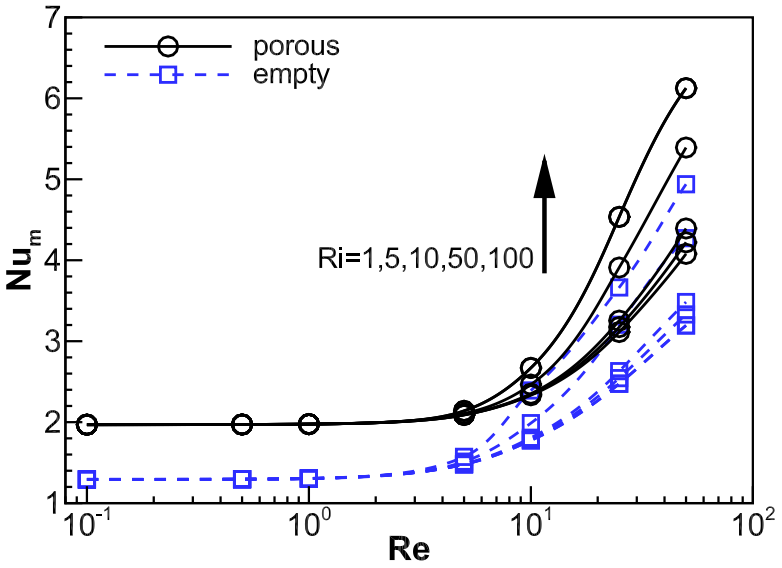

Fig. 7. Variation of Nu_m with Re at different Ri, in both empty and porous channels.

Table 1
Meshes employed to test the mesh independency.

Mesh	$(\Delta x \times \Delta y)$
$M1$	(164 × 21)
$M2$	(164 × 31)
$M3$	(164 × 41)
$M4$	(164 × 51)
$M5$	(164 × 61)
$M6$	(164 × 71)

3. Numerical approach

The dimensionless governing differential Eqs. (6)–(9), describing the evolution of the momentum and energy transport of the transient mixed convective flow in the channel, were discretised employing the finite volume method developed by Patankar [36]. This method was incorporated and used in our in-house FORTRAN code. In the beginning, the computational zone is wholly divided into spaced lines in both horizontal and vertical directions producing the primary computational mesh. The spacing of the primary mesh used here is non-uniform in the regions that experience large gradients especially close to solid boundaries and the heat source in the middle, as shown in Fig. 2a. The intersections between the horizontal and vertical lines are called grid nodes. Each gird node is surrounded by a control volume, which has boundaries located in the middle between the neighbouring nodes namely; north N, south S, east E, and west W nodes. The locations of these boundaries generate another secondary mesh called staggered mesh. Fig. 2b displays a typical control volume with dimensions ($\Delta x \times \Delta y$) surrounding a grid node P communicating with four neighbouring nodes N, S, E, W, also the staggered locations. The scalar variables, i.e., temperature and pressure, are calculated at the primary grid nodes, while the velocity components are calculated at the staggered grid locations. Then, the aforementioned Eqs. (6)–(9) are integrated over the computational grid employing the Hybrid differencing scheme described in Ferziger and Peric [37] for developing non-linear algebraic equations. After that, the SIMPLEC algorithm of Patankar [36] is employed to couple the momentum with the continuity approximations, and the alternating direction implicit (ADI) technique is used to solve them iteratively within the whole computational grid, calculating the velocities and the temperatures. The time step was carefully selected (Δt=10^{-5}) such that the numerical stability is ensured and the solution accuracy is guaranteed. In the current investigation, the convergence of the numerical solution is approached when the changes in the calculated velocity and temperature, as well as the mean Nusselt numbers Nu_m are less than (10^{-6}) over two consecutive time steps. A grid resolution study was performed to secure that the results obtained are not a function of the computational mesh. Six mesh sizes $M1$, $M2$, $M3$, $M4$, $M5$, and $M6$, shown in Table 1, were employed in the study. This study was made for the porous channel at Ri = 50 and Re = 50, and the results are shown in Fig. 3. The mesh $M4$ with 164 × 51 was chosen for the current study as it allows a reasonable compromise between the accuracy of results and the computational time cost with a maximum deviation < 0.05%.

The current numerical code was verified with the numerical results of Wong and Saeid [30] for streamlines of an air jet impingement cooling of a heat source embedded in a porous channel at Péclet number Pe=40. Fig. 4 presents the results of both algorithms. It can be seen that the figure depicts a good agreement between the two results. The current solver was also validated in our prior work (Hayder et al. [38]) for mixed convection in a square vented enclosure.

4. Results and discussion

In the current work, the fundamental investigation of the interaction between the buoyancy effects and the forced flow, in the porous and empty channels, will be first focused on. Also, the instability of the convective flow in both channels, will be checked. Then, the optimisation of the heat transfer augmentation with the pressure drop when filling the empty channel by a porous layer will be made.

Figs. 5 and 6 display the streamlines and isotherms in both empty and porous channels, at Richardson numbers Ri = 50 and 100, respectively, and for different Reynolds numbers Re = 1, 5, 10, 25, 50. Importantly to note that fixing Richardson number and increasing Reynolds number means both the forced flow effect and the heating effect increase together. For instance, at Ri = 50, when increasing Reynolds number from 1.0 to 10 means that Grashoff number increases from 50 to 5000 as $(Ri = Gr/Re^2)$, which means that both the forced flow and heating effects increase ten times together. Therefore, as can be seen in Figs. 5 and 6, for both Ri = 50 and 100, and at small Re = 1.0, although the flow intensity is low and the flow seems to be creeping, the entire field is still dominated by the forced convection due to the little range of heating, i.e. Gr = 50 and 100, respectively. However, by increasing Reynolds number, the relative strength of the buoyancy effects raises in addition to the growing in

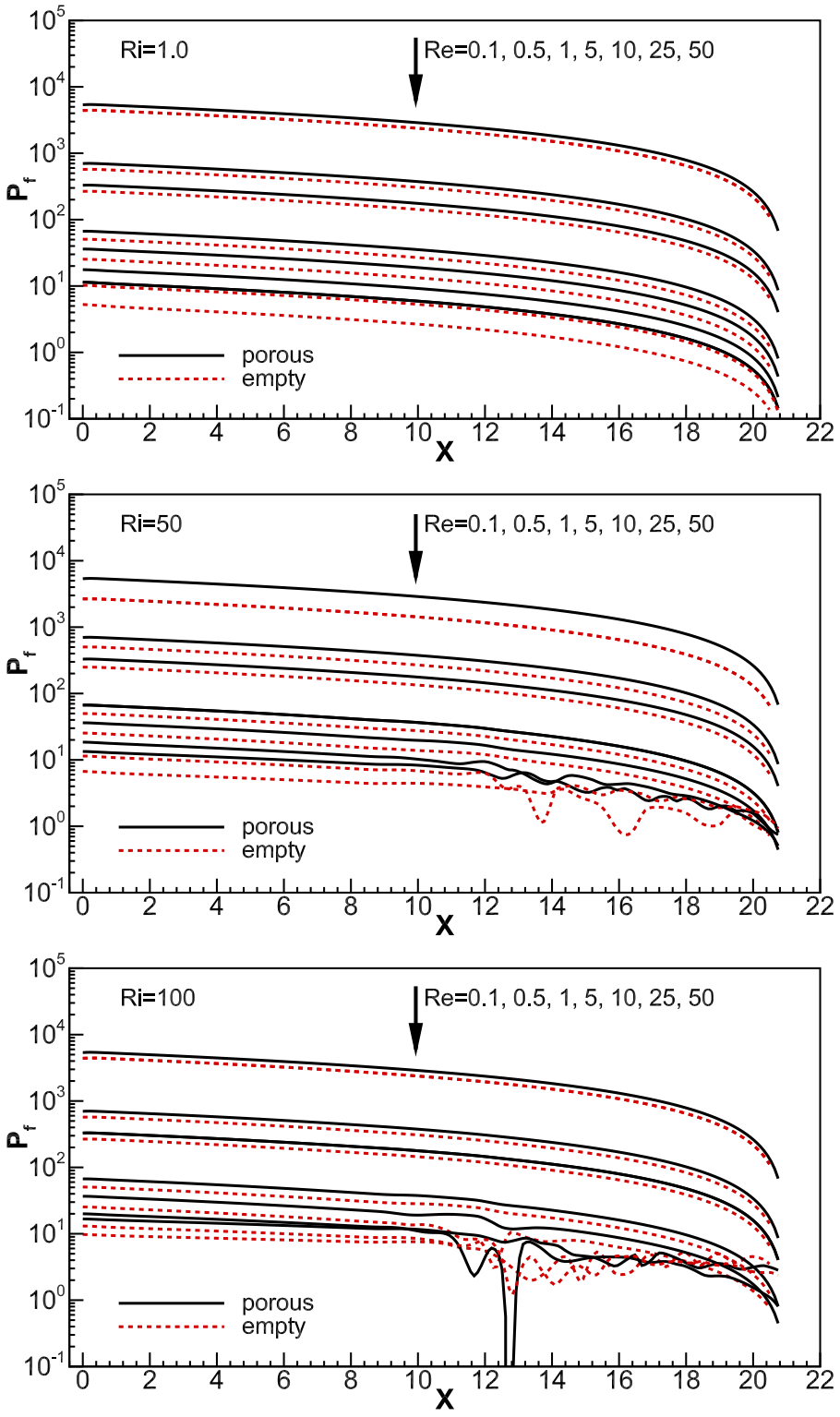

Fig. 8. Pressure distribution along both empty and porous channels at different Re, and at Ri = 1,50,100.

the intensity of the externally-induced flow. Consequently, it is shown that the temperature and velocity fields are first perturbed close to the edges of the heat element, and a pair of recirculating vortices are developed in these regions. The left cell is lifted upward attached with the top wall, whereas the right cell is forced downward attached to the bottom wall. With a further increase in Reynolds number, the forced flow relatively strengthens, resulting in that the symmetric nature of the streamlines and isotherms no longer exists, and the strength of the recirculating flows also becomes stronger. This is due to that the natural convection effect is taking over the dominance, indicating to the commencement of the mixed convection. It is also shown that the mode of mixed convection commences at earlier Reynolds numbers in the empty channel. This is because that the existence of the solid obstacles in the porous channel delay the onset of mixed convection.

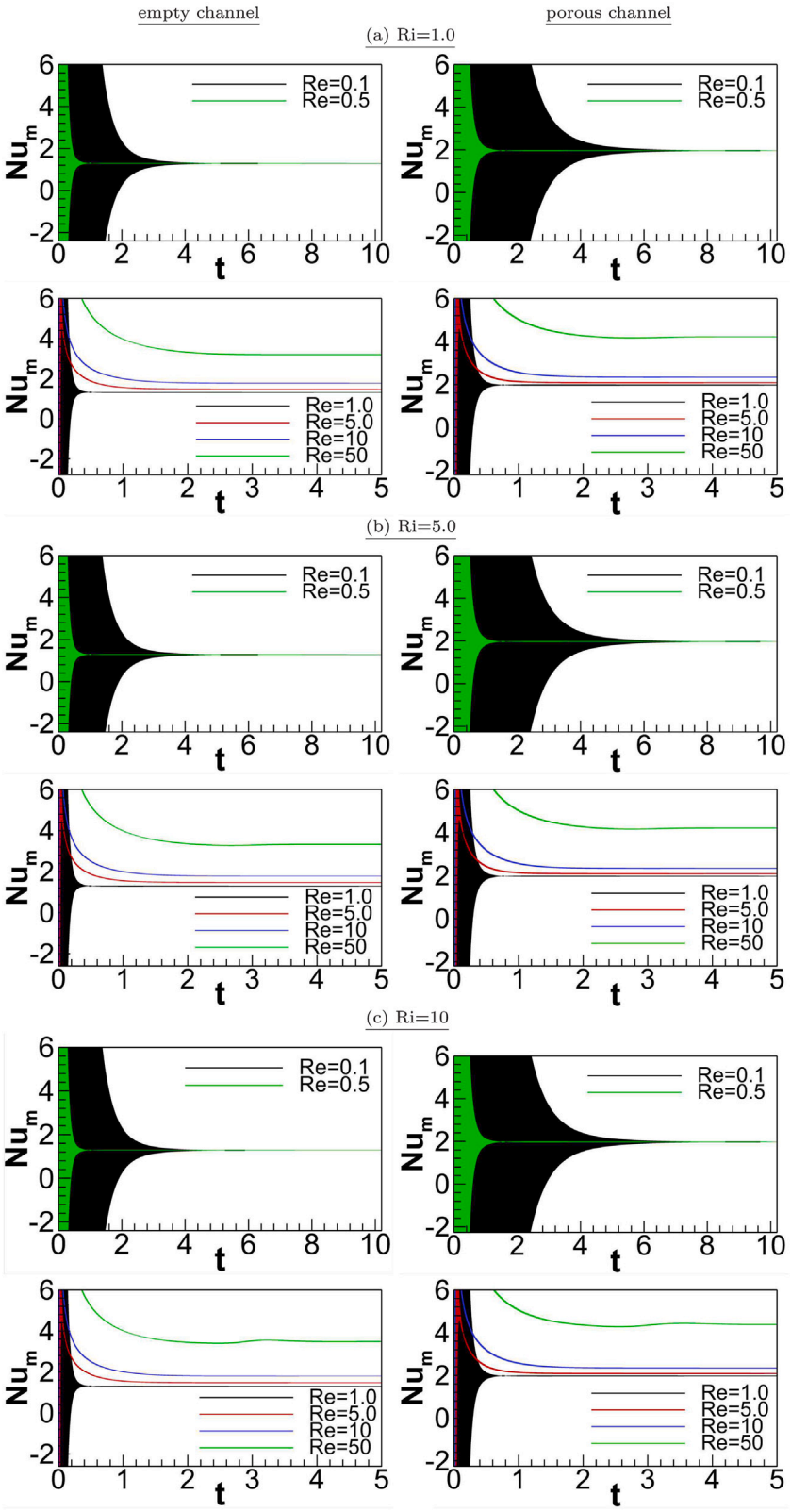

Fig. 9. Time evolution of Nu_m for increasing values of Re, at (a) Ri = 1, (b) Ri = 5, (c) Ri = 10, in (Left) empty channel, and (Right) porous channel.

For example, for Re ≥ 25, the intensity of the non-uniform re-circulating convective cells generated downstream the empty channel behind the heat source is much powerful that those in the porous channel. Once again, it is suspected that the flow for this range of Reynolds number could be unstable. In the temperature field, the effect of the alteration in the flow structure is obvious on the thermal plume, which is observed to sweep away by the flowed flow.

Fig. 7 presents the variation the mean Nusselt number Nu_m with Reynolds number for different Richardson numbers, in the two empty and porous channels. The figure shows that Nu_m of the porous duct is

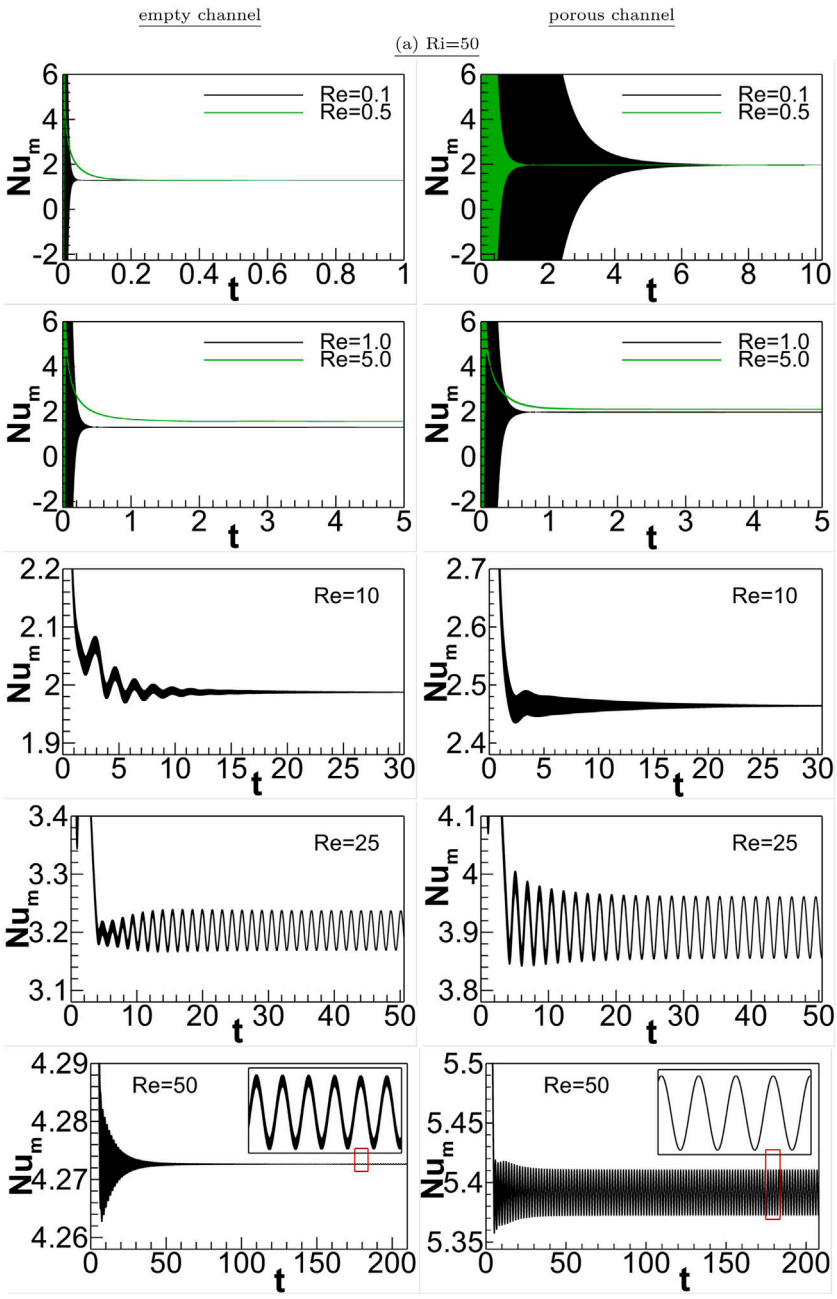

Fig. 10. Time evolution of Nu_m for increasing values of Re, at (a) Ri = 50, (b) Ri = 100, in (Left) empty channel, and (Right) porous channel.

always higher than that of the empty duct, with a difference of ≥ 70% at most due to the non-Darcy effects considered here. It demonstrates that in both channels, the trend of Nu_m remains almost constant up to Re = 5 and for all Richardson numbers; however, beyond which it increases monotonically with Reynolds number and/or Richardson number. Therefore, it can be concluded that for Re ≤ 5, Nu_m is entirely independent of both the forced flow and the buoyancy effects, and beyond which, i.e. Re > 5, Nu_m becomes a strong function of Richardson and Reynolds numbers. The reason behind this is for Re ≤ 5, the flow is very slow and does not change the thermal boundary layer formed above the heat source. Also, the thickness of this thermal boundary layer is not enlarged by increasing Richardson number due to the small space above the heat element as the channel height is small.

The pressure distributions along the length of the empty and porous channels are illustrated in Fig. 8 at different Richardson and Reynolds numbers. The results show that the pressure in both channels is decreased as Reynolds number increases, and the local pressure drops along the channel. It is also shown that the use of porous layer inside the channel may lead to a several orders of magnitude increase in the pressure due to the frictional resistance offered by the solid matrix of the porous medium. In addition, it can be seen that in both channels, although the local pressure distribution changes nearly linearly along the channel for most cases, the figure reveals that the pressure distribution shows spatial oscillating behaviours at higher Richardson and Reynolds numbers, which is an indication to an unstable behaviour. Importantly, it is also seen that the pressure gradient is inversely proportional to Reynolds number and proportional to Richardson number.

The trends of the mean Nusselt number Nu_m with time are reported in Fig. 9 for Ri = 1–10, and in Fig. 10 for Ri = 50 and 100, for different Reynolds numbers, in both empty and porous channels. The temporal variations in Fig. 9 reveal that for Ri ≤ 10, the solutions are stable for the entire Reynolds number. While, for a larger Ri ≤ 50 in Fig. 10, they exhibit an oscillatory variation as Reynolds number

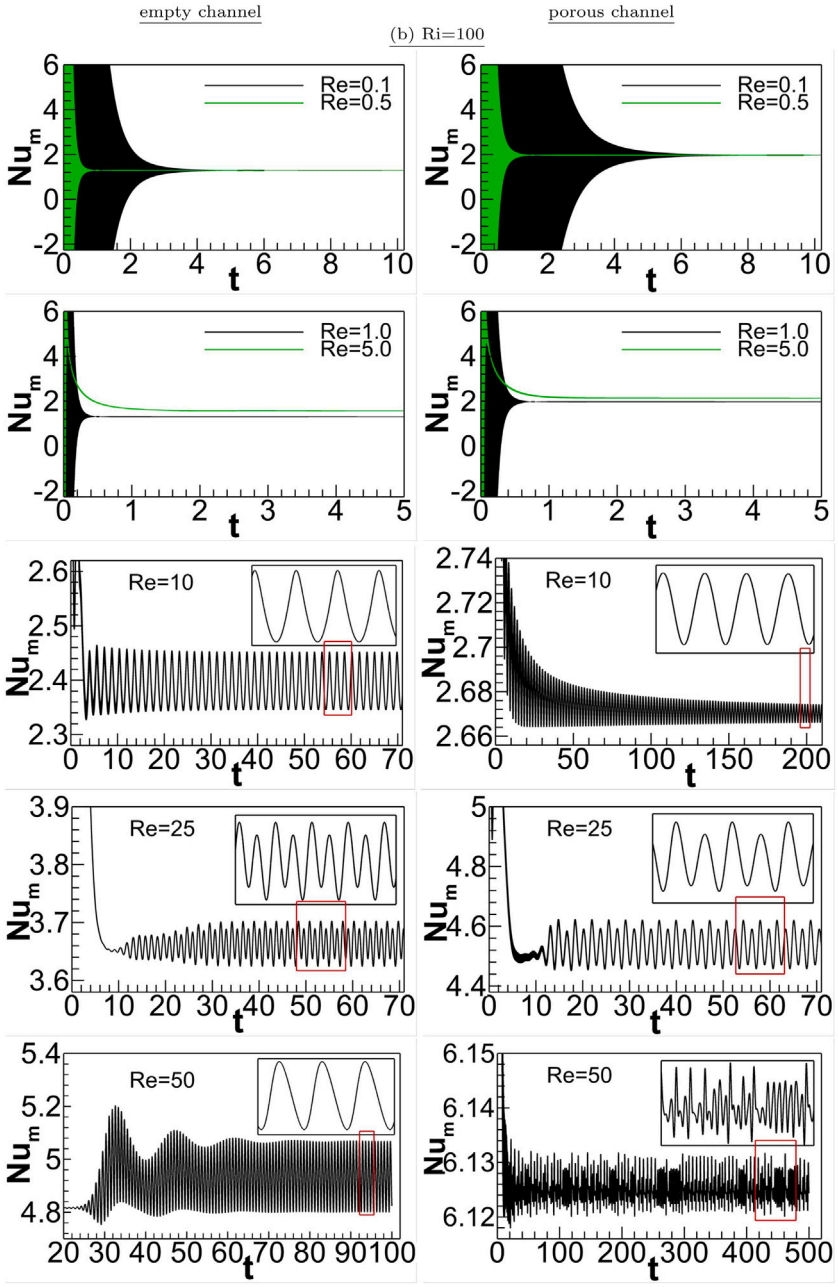

Fig. 10. (*continued*).

increases. For instance, at Ri = 50, the oscillation begins when Re ≥ 25, whereas at Ri = 100, the oscillation starts when Re ≥ 10. Indeed, this oscillatory behaviour is owing to the complicated interaction between the buoyancy effects and the forced flow in the mixed convection region. It is interesting to note that the amplitude and the period of oscillations seem to be a strong function of Richardson and Reynolds numbers. Thus, at constant Richardson number, they become considerably smaller as Reynolds number increases, and it is expected that the solution stabilises again. At this point, it is clear that the forced flow entirely predominates the buoyancy effects. However, at a constant Reynolds number, the amplitude and the period of oscillations increase as Richardson number raises, and the solution could become a random (non-fully periodic) one as at Re = 50 and Ri = 100, when the buoyancy effects suppress the forced flow.

To clarify the intricacy of the interaction between the buoyancy effects and the forced flow inside the oscillating flows, the temporal behaviour of the flow field are displayed in Figs. 11 and 12 for the two cases of when Re = 50 and Ri = 50, and when Re = 50 and Ri = 100, respectively, in the porous and empty channels. The figures demonstrate the change in the flow behaviour at 5 or 6 indicated times over fully completed oscillating periods. First, it can be seen that unstable multicellular convective flows are generated over the heat segment and behind it. Then, the flow perturbation once created is forced downstream by the external pressure-induced flow. Also, one can see that the number of cells in the empty channel are larger, and their sizes are smaller than those in the porous channel. This means that the disturbances in the empty channel is much bigger than that in the porous one. In fact, it is apparent in the figures that the flow oscillations are essentially caused by the periodic process of cell devastation and reformation with the time during the channels. In addition, it is illustrated in Fig. 12 that as Richardson number increases to 100 with keeping Re = 50, the buoyancy effects become stronger, and the flow instability becomes higher. Indeed, the mechanism behind this oscillatory performance is due to the unsteadiness of the

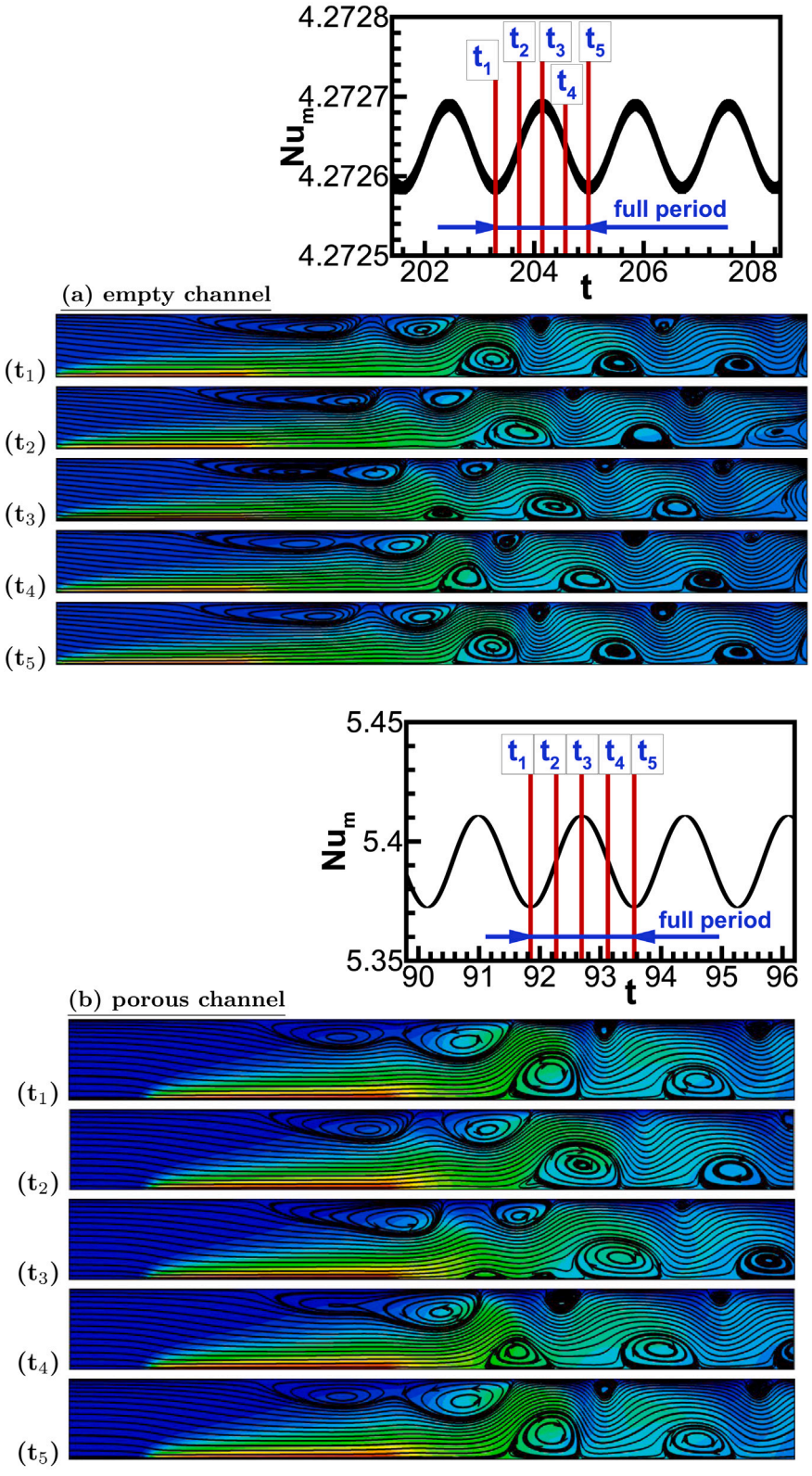

Fig. 11. Zoomed patterns of streamlines and isotherms for a periodic flow in (a) empty and (b) porous channels, at Ri = 50 and Re = 50, at indicated times over full one periodic pulse.

thermal boundary layer. Thus, the buoyancy effects incline to amplify the thermal boundary layer, whereas the forced flow attempts to suppress it.

It was shown in Figs. 7 and 8 that the increase in heat transfer acquired from inserting a porous medium inside the empty channel could be at the expense of an unfavourable increase in the pressure drop

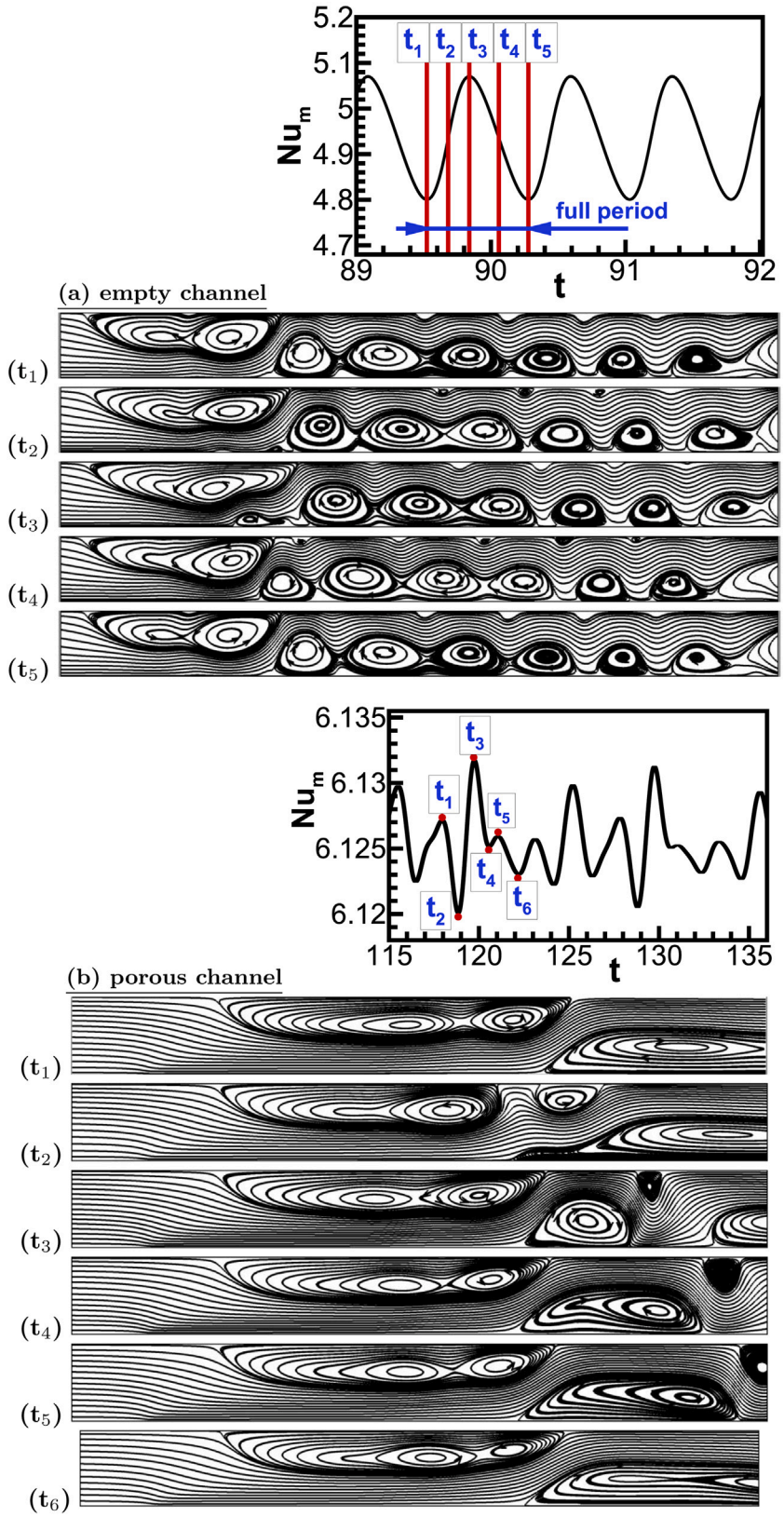

Fig. 12. Zoomed patterns of streamlines for a periodic flow in (a) empty and (b) porous channels, at Ri = 100 and Re = 50, at indicated times over full one periodic pulse.

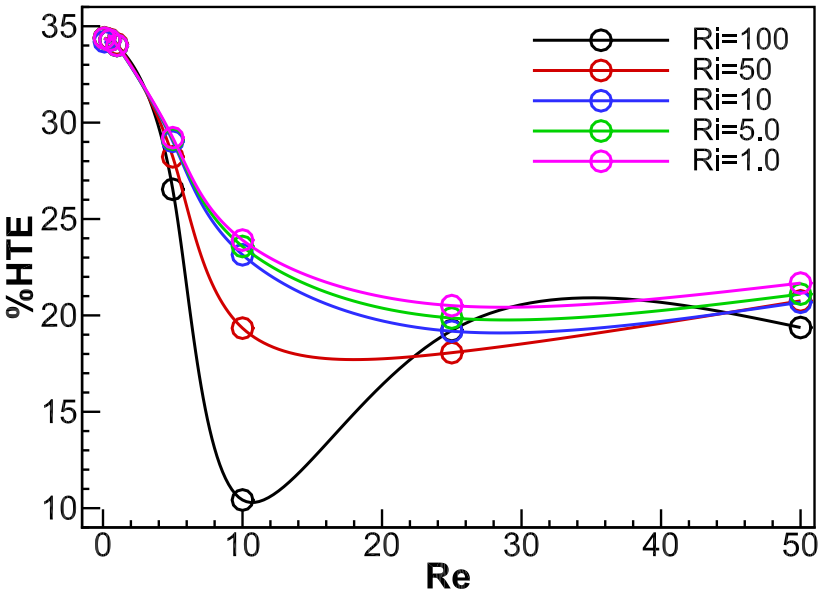

Fig. 13. Percentage of heat transfer enhancement versus Re, from the heat source due to filling the empty channel by metal fibrous material with k_r = 1000, Da = 1.0 and ε = 0.9, with Pr = 0.71 for air as a working fluid.

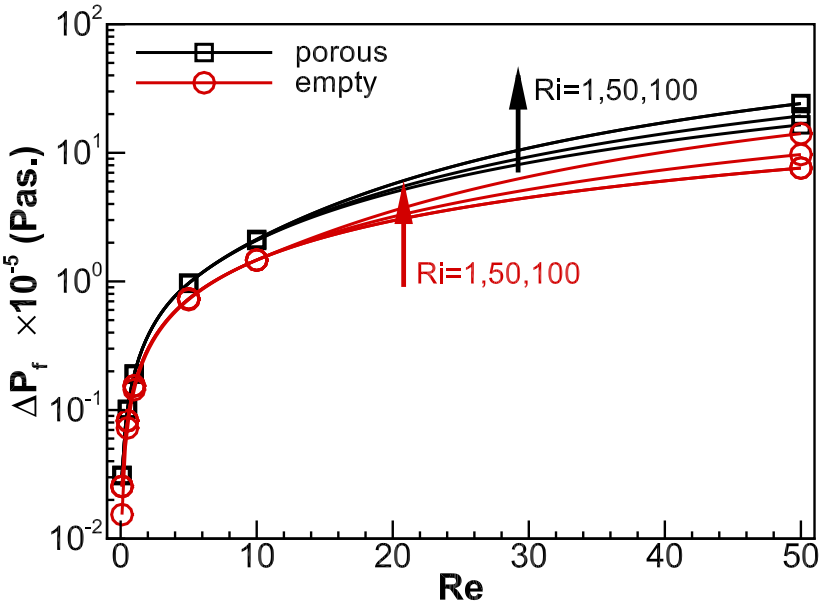

Fig. 14. Re-scaling the results of the pressure drop with Re presented in Fig. 8 for both empty and porous channels using Eq. (17).

in the porous channel. Figs. 13 and 14 present a straightforward comparison between the enhancement percentage in heat transfer (%HTE) and the pressure drop (ΔP_f) generated due to filling the empty channel by a metal fibrous material with k_r = 1000, Da = 1.0 and ε = 0.9, for the entire range of Reynolds number, and at different Richardson numbers. The value of %HTE in Fig. 13 is calculated as follows:

$$\%\mathrm{HTE} = \frac{\mathrm{Nu}_{m.porous} - \mathrm{Nu}_{m.empty}}{\mathrm{Nu}_{m.porous}} \times 100\%, \tag{16}$$

and the dimensional pressure drop in Fig. 14 is rescaled using the following equation:

$$\Delta \mathrm{P}_f = \left|\rho_f u_o^2 L\left(P_{f.out} - P_{f.o}\right)\right|. \tag{17}$$

It can be seen that %HTE approaches the maximum value around 35% at small Reynolds numbers Re ≤ 1.0, and decreases as Reynolds number increases to reach a steady value around 20% for Reynolds numbers Re ≥ 20. This is for all heating conditions except at Ri = 100, in which %HTE drops significantly from the peak to a minimum value 11% at Re = 10, and then increases to the steady value 20%. The reason behind the reduction in %HTE as Reynolds number increases is that the difference in Nu_m in both porous and empty channels is bigger for lower Reynolds numbers when Nu_m remains unchanged, see Fig. 7, and this difference getting slightly smaller as Reynolds number increases when the channel enters the mode of mixed convection. However, this overall achievement in %HTE is plausible and can be the need in several thermal applications.

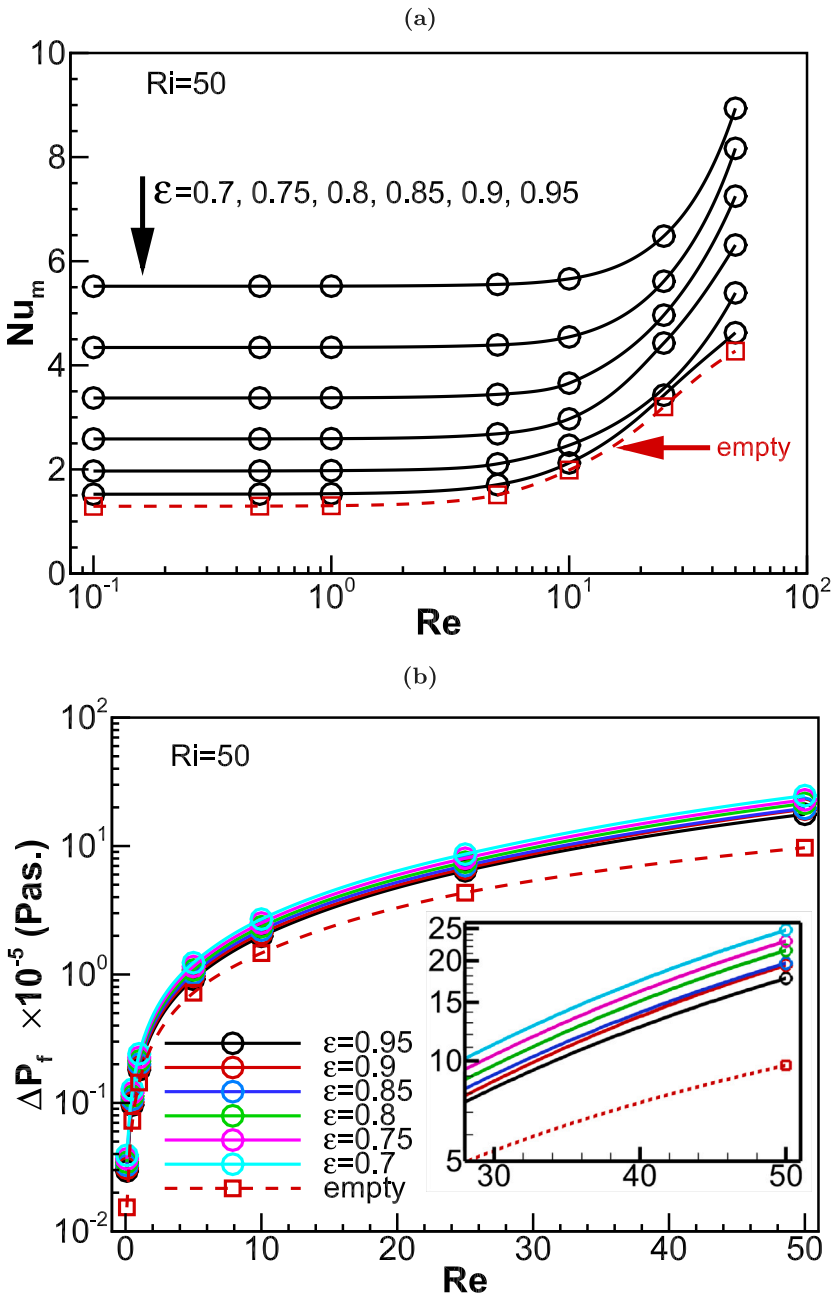

Fig. 15. Variations of (a) Nu_m and (b) re-scaled pressure drop ΔP_f, with Re at different porosity ε of fibrous channel, at k_r = 1000, Da = 1.0, and compared with empty channel, at Ri = 50.

Against this advantage in %HTE, a significant increase in ΔP_f, e.g., several hundred fold compared with the empty channel, is produced. This is due to the high level of frictional resistance offered by the solid substances of the porous medium used. In fact, this increase in ΔP_f when filling the channel with a porous material requires a huge mechanical power for pumping, especially for higher Reynolds numbers, which can be undesirable in the design of heat exchangers. Therefore, in this study, these two parameters, %HTE and

ΔP_f, will be further probed at different conditions, e.g., different structural properties of the porous medium, to detect the optimal circumstances for increasing $\%HTE$ and reducing ΔP_f.

Fig. 15 displays the variations of Nu_m and the pressure drop ΔP_f against Reynolds number at variant values of porosity of the porous medium used, ε = 0.7–0.95, at constant Ri = 50 and Da = 1.0. The results that are reported in this figure are compared with those for the empty channel, e.g. ε = 1.0. Obviously, it is shown that Nu_m decreases as the porosity increases, revealing that more heat transfer can be obtained by utilising porous media with lower porosity. Indeed, in porous media, larger porosity means the content of the solid matrix in less. Consequently, the interfacial contact area between the stationary solid phase and the flowing fluid phase is less. This effect decreases the energy exchange between the two phases, and leads to a lower heat transfer from the heat source, e.g. lower Nu_m. Moreover, the figure reveals that ΔP_f also decreases with an increase in the porosity. This is expected as less solid content results in a stronger reduction in the flow resistance and pressure drop. For instance, it reduces from $\sim 0.03911 \times 10^{-5}$ (pas.) to $\sim 0.02948 \times 10^{-5}$ (pas.) (~1.32 times) as the porosity increases from 0.7 to 0.95 at Re = 0.1, and from $\sim 24.6891 \times 10^{-5}$ (pas.) to $\sim 17.6812 \times 10^{-5}$ (pas.) (~1.4 times) at Re = 50. Percentages of heat transfer enhancement %HTE and pressure drop reduction $\%\Delta P_f$ as the

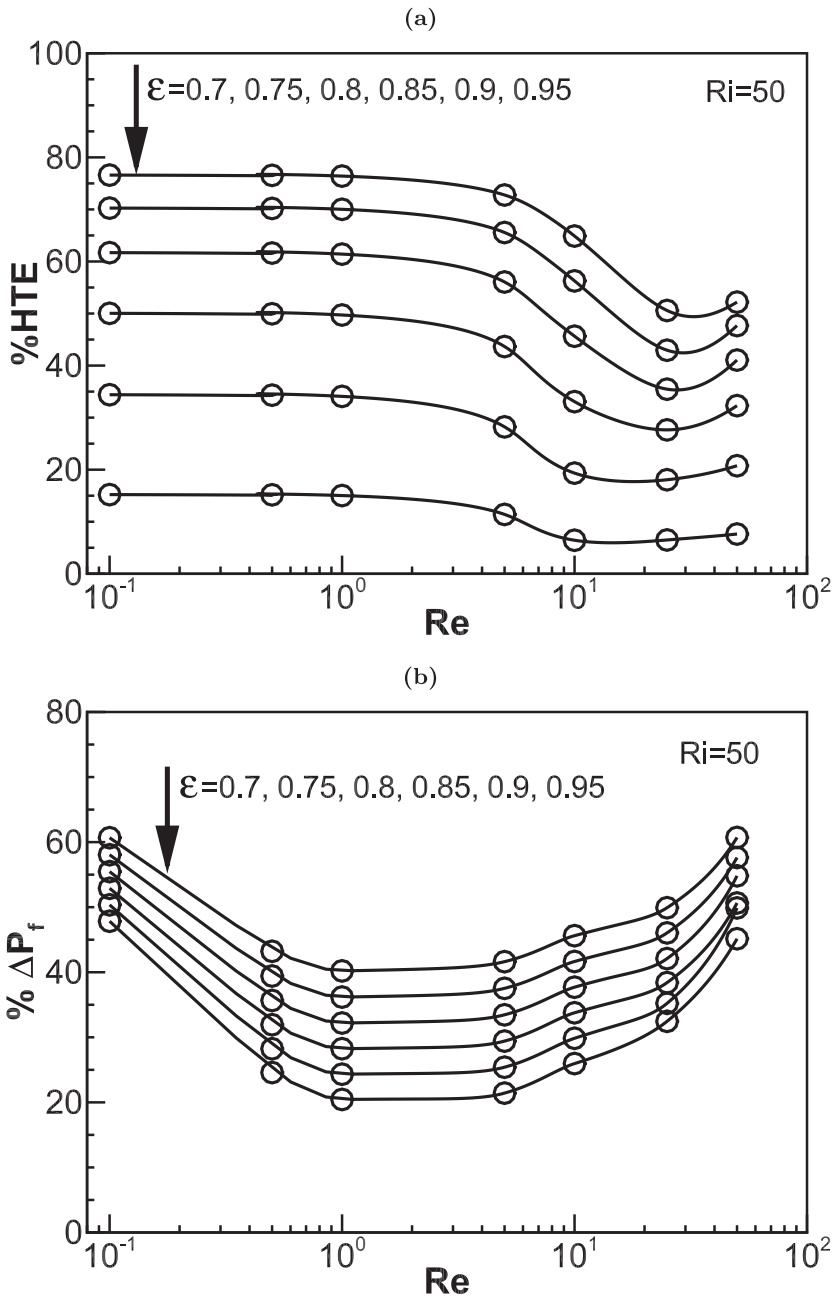

Fig. 16. Percentage of (a) heat transfer enhancement and (b) pressure drop, throughout the fibrous channel, against Re for different porosity ε, at k_r = 1000, Da = 1.0, and compared with empty channel, at Ri = 50.

porosity changes over the range of ε = 0.7–0.95 are displayed in Fig. 16. The value of $\%\Delta P_f$ is calculated as follows:

$$\%\Delta P_f = \frac{\Delta P_{f.porous} - \Delta P_{f.empty}}{\Delta P_{f.porous}}. \quad (18)$$

Importantly, it is found that for Re = 0.1–1.0, %HTE decreases from ~78% to ~18% (with ~50% ↓ reduction) as the porosity increases from ε = 0.7 to 0.95, while $\%\Delta P_f$ decreases from ~62% to ~45% (with ~17% ↓ reduction). Also, at Re = 50, %HTE decreases from ~58% to ~16% (with ~48% ↓ reduction) as the porosity increases from ε = 0.7 to 0.95, while $\%\Delta P_f$ decreases from ~62% to ~42% (with ~20% ↓ reduction). This means that the moderate value of porosity, e.g. ε = 0.7–0.8, is beneficial for obtaining higher %HTE and relatively lower $\%\Delta P_f$.

The effect of changing the permeability of the porous medium represented by Darcy number on Nu_m and the pressure drop ΔP_f is shown in Fig. 17, for different Reynolds number and at constant k_r = 1000, ε = 0.9, and Ri = 50. It is worth mentioning that low Darcy number means that the conduction heat transfer is predominated, and the porous medium provides a significant resistance to the buoyancy effects; however, as Darcy number increases, the fluid flow becomes less restrictive, consequently the heat transfer turns to be convection-dominated, and the solution approaches the clear fluid. Importantly, the figure shows that the heat transfer in the existence of the porous medium is overall much better than that in the empty channel, with much less hydraulic resistance. In addition, in the porous channel, it is shown that for Re≤1.0, e.g. natural convection is dominated, changing the Darcy number form small to high values generates insignificant alterations in the overall Nusselt number, but increasing Darcy number can only reduce the hydraulic resistance and the pressure drop considerably. However, for higher Reynolds numbers, i.e. Re>1.0,

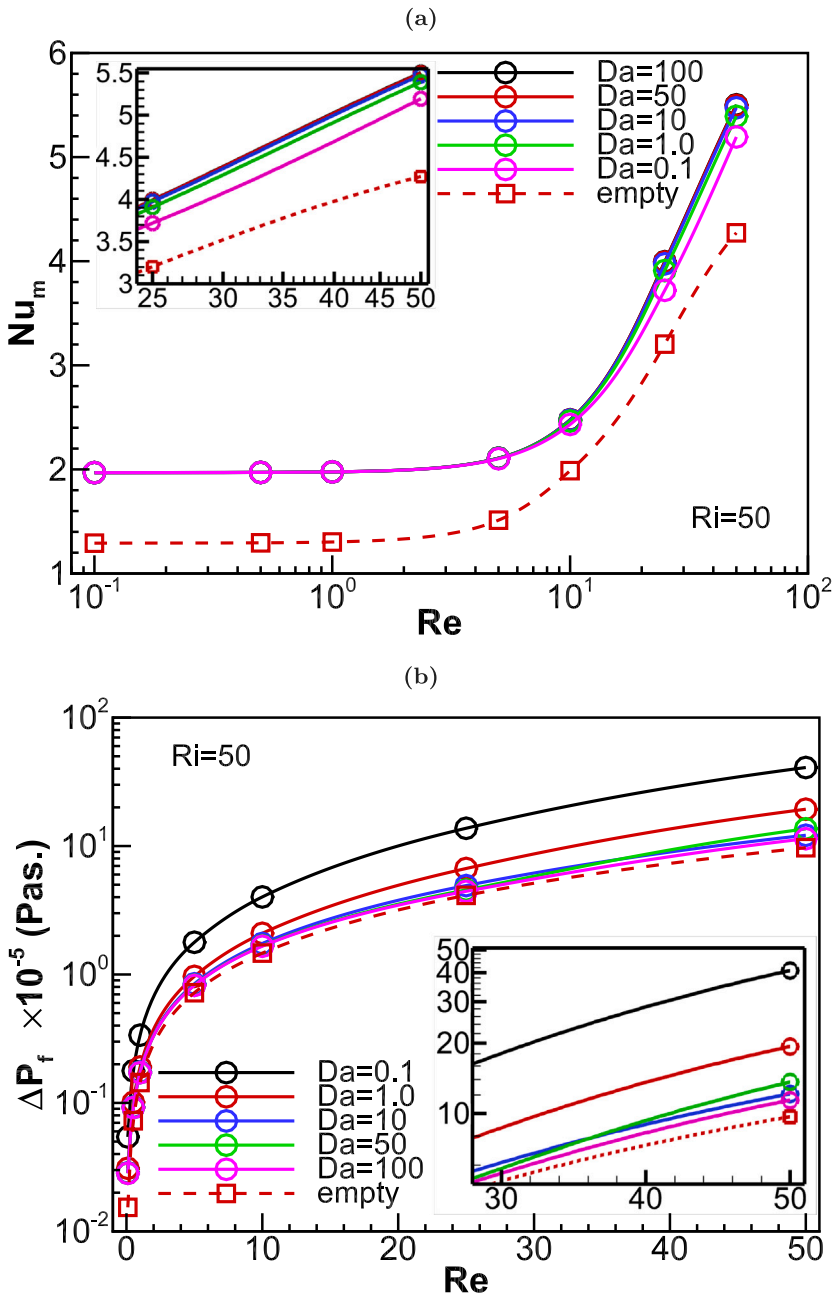

Fig. 17. (a) Variation of Nu_m and (b) Percentage of heat transfer enhancement, with Re at different Da of fibrous channel, at k_r = 1000, ϵ = 0.9, and compared with empty channel, at Ri = 50.

the increase in Darcy number causes a little raise in heat transfer and a significant reduction in the pressure drop. Fig. 18 displays the percentages of heat transfer enhancement %HTE and pressure drop reduction $\%\Delta P_f$ as Darcy number is varied. It can be seen that Darcy number does not change %HTE for Re≤1.0; however, for Re> 1.0%HTE increases slightly as Darcy number increases. For example, it increases from ~ 18.5% to ~20%, from ~14% to ~ 20.5%, and from ~17% to ~ 22.5%, as Darcy number increases from 0.1 to 100, at Re = 10, 25 and 50, respectively. Whereas, $\%\Delta P_f$ reduces significantly as Darcy number increases. For example, it decreases from ~72% to ~46%, from ~58% to ~17%, from ~65% to ~12% and from ~77% to ~15%, as Darcy number increases from 0.1 to 100, at Re = 0.1, 1.0, 10 and 50, respectively.

5. Conclusions

Numerical results are reported for unsteady combined forced and natural convection over a horizontal porous layer confined by two impermeable plates with a localised heating from below when the heat source length equals to three times the layer height $S = 3H$. The results show that the flow and thermal fields exhibit oscillatory behaviours at higher Richardson number and/or higher Reynolds number, and the amplitude and period of oscillations are strongly dependent on these numbers. Thus, when the mixed convection commences, unstable multiple non-uniform recirculating convective cells are developed downstream the channel, and the flow instability in the empty duct is bigger than that in the porous duct. The existence of the porous material enhances the heat transfer considerably at most; however, the

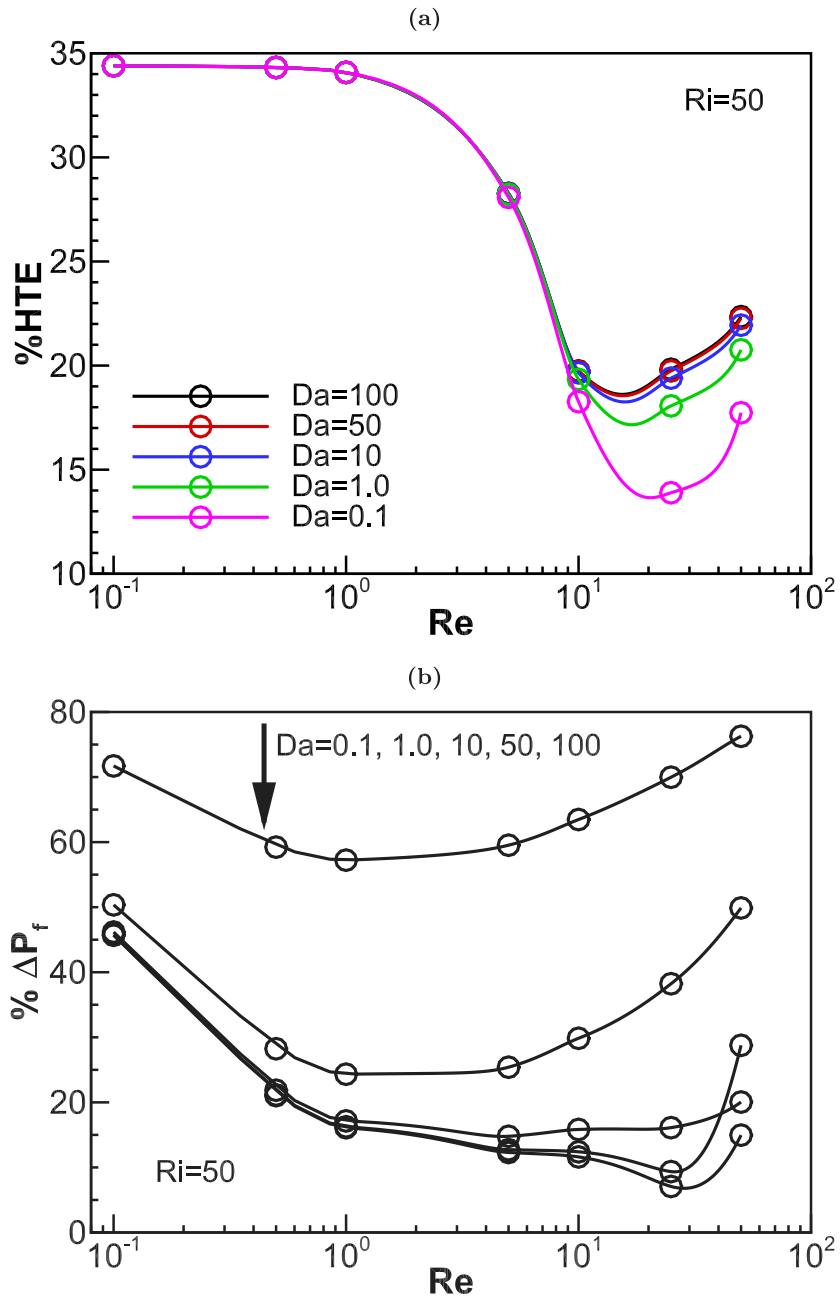

Fig. 18. Percentage of (a) heat transfer enhancement and (b) pressure drop, throughout the fibrous channel, against Re for different Da, at k_r = 1000, ε = 0.9, and compared with empty channel, at Ri = 50.

pressure drop is also increased significantly. Both the heat transfer and the pressure drop are decreased as the porosity increases. However, the reduction in heat transfer enhancement is quite greater than that in the pressure drop, which means that moderate values of porosity are desirable for both of good enhancement in heat transfer and better reduction in pressure drop. The effect of Darcy number is much less than the porosity effect. Thus, for low Reynolds number, Darcy number has almost negligible impact on the heat transfer enhancement and the reduction in pressure drop. However, for higher Reynolds number, the increase in Darcy number increases slightly the heat transfer augmentation and lessens dramatically the reduction in pressure drop.

Nomenclature

C_F	inertia coefficient
Da	Darcy number, Da = K/H^2
g	gravitational acceleration, (m/s^2)
Gr	Grashof number, $Gr = g.\beta.\rho^2.H^3.(T_h - T_o)/\mu^2$
h_x	local convective heat transfer coefficient, (W/m^2 K)
H	channel height, (m)
k	thermal conductivity, (W/m K)
k_r	thermal conductivity ratio, (k_s/k_f)
K	permeability, (s/m)
L	channel length, (m)
Nu_l	local Nusselt number

Nu_m	mean Nusselt number
p_f	dimensional pressure, (N/m^2)
P_f	non-dimensional pressure, $P_f = p_f/\rho.u_o^2$
Re	Reynolds number, $Re = u_o.\rho_f.H/\mu$
Ri	Richardson number, $Ri = Gr/Re^2$
S	length of heat source, (m)
T	dimensional temperature, (C^o)
t'	dimensional time, (sec)
t	non-dimensional time, $t = t'/u_oH$
u, v	dimensional flow velocities, (m/s)
U, V	non-dimensional group of velocities
x, y	dimensional Coordinates, (m)
X, Y	non-dimensional coordinates, $X = x/H$, $Y = y/H$

Greek symbols

α_r	thermal diffusivity ratio, (α_s/α_f)
β	coefficient of volumetric expansion
θ	non-dimensional temperature, $\theta = (T - T_o)/(T_h - T_o)$
ρ_f	density, (kg/m^3)
ε	porosity
μ	fluid dynamic viscosity, (N s/m^2)

Subscripts

eff	effective
f	fluid
h	hot
l	local
m	mean
n	perpendicular
o	inlet
out	outlet
r	ratio
s	solid
w	wall

CRediT authorship contribution statement

Suha A. Mohammed: Writing – original draft, Resources. **Gazy F. Al-Sumaily:** Conceptualization, Data curation, Formal analysis, Writing – review & editing. **Hayder A. Dhahad:** Methodology, Validation, Investigation, Visualization. **Mark C. Thompson:** Software, Supervision, Project administration.

Declaration of competing interest

The authors declare that they have no known competing financial interests or personal relationships that could have appeared to influence the work reported in this paper.

Acknowledgements

This research was supported in part by the Monash eResearch Centre and eSolutions-Research Support Services through the use of the MonARCH HPC Cluster.

Funding

This research did not receive any specific grant from funding agencies in the public, commercial, or not-for-profit sectors.

References

[1] H. Hadim, G. Chen, Non-darcy mixed convection in a vertical porous channel with asymmetric wall heating, J. Thermophys. Heat Trans. 8 (4) (1994) 805–808.
[2] Y.C. Chen, J.N. Chung, C.S. Wu, Y.F. Lue, Non-Darcy mixed convection in a vertical channel filled with a porous medium, Int. J. Heat Mass Transfer 43 (13) (2000) 2421–2429.
[3] Y.J. Rami, A.B. Fawzi, A. Fahmi, Darcy-Forchheimer mixed convection heat and mass transfer in fluid saturated porous media, Int. J. Numer. Methods H 11 (5/6) (2001) 600–618.
[4] G. Degan, P. Vasseur, Aiding mixed convection through a vertical anisotropic porous channel with oblique principal axes, Internat. J. Engrg. Sci. 40 (2) (2002) 193–209.
[5] I. Pop, D.A.S. Rees, C. Egbers, Mixed convection flow in a narrow vertical duct filled with a porous medium, Int. J. Therm. Sci. 43 (5) (2004) 489–498.
[6] J.C. Umavathi, J.P. Kumar, A.J. Chamkha, I. Pop, Mixed convection in a vertical porous channel, Transp. Porous Media 61 (3) (2005) 315–335.
[7] B. Buonomo, O. Manca, P. Mesolella, S. Nardini, Local thermal non-equilibrium in mixed convection in channels partially heated at uniform heat flux filled with a porous medium, in: Proceedings of the ASME 2014 12th Biennial Conference on Engineering Systems Design and Analysis ESDA2014, vol. 3, Copenhagen, Denmark, 2014, pp. ESDA2014–20538.
[8] A.A. Avramenko, Y.Y. Kovetska, I.V. Shevchuk, A.I. Tyrinov, V.I. Shevchuk, Mixed convection in vertical flat and circular porous micro-channels, Transp. Porous Media 124 (2018) 919–941.
[9] M. Izadi, P.S.M.R. Hashemi, A.K. Yasuri, A.J. Chamkha, Mixed convection of a nanofluid in a three-dimensional channel, J. Therm. Anal. Calorim. 136 (2019) 2461–2475.
[10] B. Kotresha, N. Gnanasekaran, Determination of interfacial heat transfer coefficient for the flow assisted mixed convection through brass wire mesh, Int. J. Therm. Sci. 138 (2019) 98–108.
[11] B. Kotresha, N. Gnanasekaran, C. Balaji, Numerical simulations of flow-assisted mixed convection in a vertical channel filled with high porosity metal foams, Heat Transfer Eng. 41 (8) (2020) 739–750.
[12] V. Leela, K.N. Seetharamu, N. Kotloni, R.G. Reddy, Effect of asymmetrical wall heat flux and wall temperature ratio on mixed convection in a vertical micro-porous-channel with internal heat generation, Propuls. Power Res. 9 (4) (2020) 394–407.
[13] K.K. Manish, K.S. Abhishek, P. Bera, Instability of mixed convection in a differentially heated channel filled with porous medium: A finite amplitude analysis, Phys. Fluids 33 (2021) 024109.
[14] B.M. Shankar, J. Kumar, I.S. Shivakumara, Numerical investigation of the stability of mixed convection in a differentially heated vertical porous slab, Appl. Math. Comput. 389 (2021) 125486.
[15] F.C. Lai, V. Prasad, F.A. Kulacki, Effects of the size of heat source on mixed convection in horizontal porous layers heated from below, in: Proceedings of the 2nd ASME-JSME Thermal Engineering Joint Conference, vol. 2, American Society of Mechanical Engineers, Honolulu, Hi, USA, 1987, pp. 413–419.
[16] V. Prasad, F.C. Lai, F.A. Kulacki, Mixed convection in horizontal porous layers heated from below, J. Heat Trans-T ASME 110 (2) (1988) 395–402.
[17] F.C. Chou, P.Y. Chung, Effect of stagnant conductivity on non-darcian mixed convection in horizontal square packed channels, Numer. Heat Transf. A 27 (2) (1995) 195–209.
[18] Y. Yokoyama, F.A. Kulacki, R.L. Mahajan, Mixed convection in a horizontal porous duct with a sudden expansion and local heating from below, J. Heat Trans.-T ASME 121 (3) (1999) 653–661.
[19] P.Y. Chang, S.W. Shiah, M.N. Fu, Mixed convection in a horizontal square packed-sphere channel under axially uniform heating peripherally uniform wall temperature, Numer. Heat Transf. A 45 (8) (2004) 791–809.
[20] D. Cimpean, I. Pop, D.B. Ingham, J.H. Merkin, Fully developed mixed convection flow between inclined parallel plates filled with a porous medium, Transp. Porous Media 77 (2009) 87–102.
[21] K.C. Wong, N.H. Saeid, Numerical study of non-darcian effects on jet impingement cooling in a horizontal porous layer in the mixed convection regime, Int. Commun. Heat Mass Transf. 36 (1) (2009) 45–50.
[22] J.M. Dixon, F.A. Kulacki, Mixed convection in fluid-superposed porous layers. Part 2: Experiments, Int. J. Heat Mass Transfer 109 (2017) 1301–1306.
[23] J.M. Dixon, F.A. Kulacki, Mixed convection in fluid superposed porous layers. Part 1: Analysis, Int. J. Heat Mass Transfer 109 (2017) 1289–1300.
[24] F. Ozgen, V. Yasin, Numerical study of mixed convection in a channel filled with a porous medium, Appl. Sci. 9 (2) (2019) 211–223.
[25] A. Barletta, D.A.S. Rees, Unstable mixed convection flow in a horizontal porous channel with uniform wall heat flux, Transp. Porous Media 129 (2019) 385–402.
[26] A. Barletta, M. Celli, P.V. Brandão, L.S. de B. Alves, Wavepacket instability in a rectangular porous channel uniformly heated from below, Int. J. Heat Mass Transfer 147 (2020) 118993.
[27] B. Buonomo, V. Fardella, M. Manca, S. Nardini, S. Vigna, Investigation on thermal and fluid dynamic behaviors in mixed convection in horizontal channels with aluminium foam and heated from below, in: E3S Web Conf., vol. 197, 75° National ATI Congress, 2020, p. 10006.
[28] F.C. Lai, F.A. Kulacki, Transient mixed convection in horizontal porous layers locally heated from below, in: ASME Proceedings of the 1988 National Heat Transfer Conference, vol. 96, Houston, TX, USA, 1988, pp. 353–364.
[29] N.H. Saeid, I. Pop, Periodic mixed convection in horizontal porous layer heated from below by isoflux heater, Arab J. Sci. Eng. 31 (2B) (2006) 153–164.
[30] K.C. Wong, N.H. Saeid, Numerical study of mixed convection on jet impingement cooling in a horizontal porous layer under local thermal non-equilibrium conditions, Int. J. Therm. Sci. 48 (5) (2009) 860–870.
[31] M. Kaviany, Principles of Heat Transfer in Porous Media, Springer-Verlag, 1995.
[32] D.A. Nield, A. Bejan, Convection in Porous Media, third ed., Springer Science+Business Media, New York, NY, USA, 2006.

[33] H.A. Wissam, F.A. Gazy, A.D. Hayder, C.T. Mark, Numerical analysis of non-darcian mixed convection flows in a ventilated enclosure filled with a fluid-saturated porous medium, TSEP 24 (2021) 100922.
[34] P. Zehner, E.U. Schluender, Thermal conductivity of granular materials at moderate temperatures, Chemie-Ingenieur-Technik 42 (14) (1970) 933–941.
[35] S. Ergun, Fluid flow through packed columns, Chem. Eng. Prog. 48 (2) (1952) 89–94.
[36] S.V. Patankar, Numerical Heat Transfer and Fluid Flow, Hemisphere Publishing Corporation, New York, 1980.
[37] J.H. Ferziger, M. Peric, Computational Methods for Fluid Dynamics, Springer, Berlin, 1997.
[38] A.D. Hayder, F.A. Gazy, H.A. Wissam, C.T. Mark, Aiding and opposing re-circulating mixed convection flows in a square vented enclosure, TSEP 19 (2020) 100577.